International Journal of Fracture **65**: 277–290, 1994.

Smeared-tip superposition method for cohesive fracture with rate effect and creep

ZDENĚK P. BAŽANT and STEPHEN BEISSEL
Northwestern University, Evanston, Illinois 60208, U.S.A.

Received 9 February 1993; accepted in revised form 13 July 1993

Abstract. A recent formulation of the smeared-tip superposition method presented by Bažant [1], which itself was a generalization and modification of an integral equation formulation with an asymptotic series solution derived by Planas and Elices [2], is further improved, generalized and adapted to an efficient finite difference solution scheme. A crack with bridging stresses is modeled as a superposition of infinitely many LEFM cracks with continuously distributed (smeared) tips having infinitely small intensity factors. Knowledge of the stress intensity factor as a function of the location of the crack tip along the crack path is all that is needed to obtain the load-displacement relation. The solution is reduced to a singular integral equation for a function describing the components of applied load associated with crack tips at various locations. The integral equation is complemented by an arbitrary relation between the bridging stress and the crack opening displacement, which can be rate-independent or rate-dependent. Furthermore, using the creep operator method, the equation is extended to aging linearly viscoelastic behavior in the bulk of the specimen. The previously presented finite difference solution is improved and generalized in a form that leads to a system of nonlinear algebraic equations, which can be solved by an optimization method. Application of the smeared-tip method to the analysis of recent measurements of the size effect in three-point-bend fracture specimens of different sizes is presented and a crack opening law that yields the main qualitative characteristics of the test results, particularly an increase of brittleness with a decreasing loading rate, is presented.

1. Introduction

If the entire structure behaves linearly except for nonlinear behavior at the crack line, the load-displacement relation can be calculated solely on the basis of knowing the stress intensity factor as a function of the crack length. In recognition of this fact, a new method for nonlinear fracture behavior with bridging stresses as well as the rate effect and creep was proposed in [1], as an extension of an ingenious integral equation previously presented by Planas and Elices [2, 3]. This method can be applied to arbitrary nonlinear material behavior in the crack bridging zone and to time-dependent behavior in this zone coupled with aging linearly viscoelastic behavior in the rest of the structure.

In this method, the solution for a cohesive crack (crack with bridging stresses) is expressed as a superposition of the exact solutions of linear elastic fracture mechanics (LEFM) for crack tips at various locations along the crack line. The tips of these LEFM cracks are continuously distributed (smeared) along the crack line. Their stress intensity factors are infinitely small but their superposition yields a finite density of the stress intensity factor along the crack line. While Planas and Elices [2, 3] used an asymptotic series expansion to solve the integral equation resulting from the superposition of infinitely many LEFM cracks, a method of solving more general integro-differential equations by means of the finite differences was presented by Bažant [1]. Numerical applications though, have not been demonstrated.

The purpose of this paper is to present an improved version of the smeared-tip method and demonstrate its application to rate-dependent fracture of concrete specimens exhibiting creep. The improvement of the method will consist of

(1) using a different function for characterizing the density of LEFM cracks in a manner that removes singularity at the initial crack (notch) tip, and

(2) developing a more effective and more general finite difference formulation in which the resulting system of nonlinear algebraic equations can be solved by an optimization technique.

2. Linear elastic fracture mechanics relations for a single crack

We need to begin by a brief exposition of the smeared-tip method from [1]. The basic relation is the following well-known expression for the stress intensity factor K for a crack of length s in a two-dimensional elastic structure (e.g. Broek [4])

$$K = \frac{Pk(\eta)}{b\sqrt{L}}, \tag{1}$$

P = applied load, L = length of the crack ligament, b = structure thickness, and $k(\eta)$ = nondimensional function of nondimensional coordinate $\eta = s/L$ where s = coordinate of the crack tip (Fig. 1a). We will restrict attention to mode I (opening mode) fracture, although the present method could equally well be applied to mode II or III (shear) fracture. The load-point displacement u may generally be calculated as (e.g. Bažant and Cedolin [5]) $u = C_0P + P\psi(\eta)/E'b$ or

$$u = \frac{P\chi(\eta)}{E'b}, \tag{2}$$

with

$$\chi(\eta) = \bar{C}_0 + \psi(\eta), \quad \psi(\eta) = 2\int_0^\eta [k(\eta')]^2 \, d\eta', \tag{3}$$

where $\bar{C}_0 = C_0E'b$, C_0 = compliance when there is no crack; $\chi(\eta)$ is a nondimensional function, which can also be obtained by LEFM (linear elastic fracture mechanics), for example by optimum fitting of the strain energy values obtained for different crack lengths with a linear elastic finite element program; and $E' = E$ = Young's modulus, for the case of plane stress, or $E' = E/(1-\nu)^2$, for the case of plane strain.

When the crack tip is at s, the LEFM solutions for the normal stress σ across the crack plane and the opening displacements v of points on the crack surfaces (representing half of the crack width) have the general form

$$\text{for} \quad \eta < \xi \le 1: \quad \sigma = \frac{P}{Lb} S(\xi, \eta), \tag{4}$$

$$\text{for} \quad 0 \le \xi \le \eta: \quad v = \frac{P}{E'b} V(\xi, \eta), \tag{5}$$

where $\xi = x/L$ and x is the coordinate along the crack line (Fig. 1). The following approximations can be used for sufficiently small $|\xi - \eta|$:

$$S(\xi, \eta) = \frac{1}{\sqrt{2\pi}} \frac{k(\eta)}{\sqrt{\xi - \eta}}, \tag{6}$$

$$V(\xi, \eta) = \sqrt{\frac{8}{\pi}} k(\eta)\sqrt{\eta - \xi}, \tag{7}$$

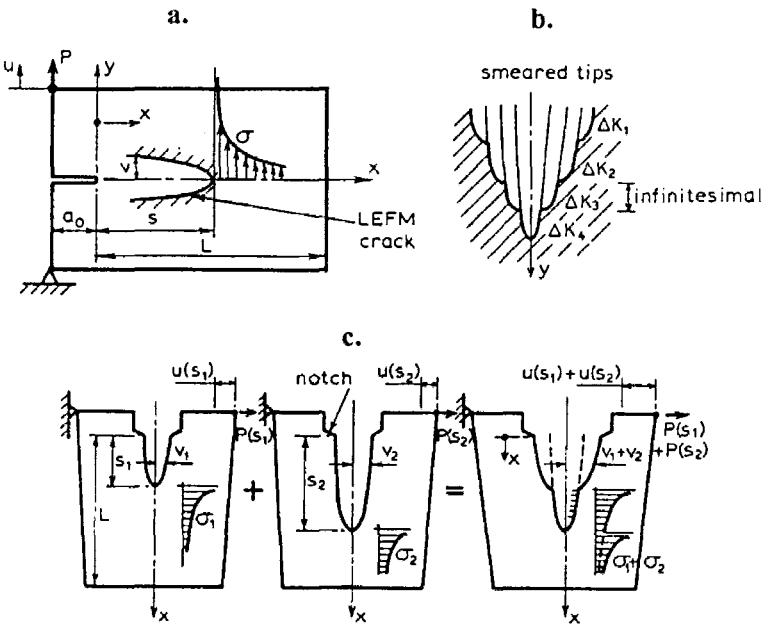

Fig. 1. (a) LEFM stress and displacement distributions for a crack tip at $x = s$; (b) Superposition of crack opening profiles of many LEFM cracks of different lengths; and (c) Superposition of crack opening displacement and stress distributions for two cracks.

(Fig. 1). When $|\ \xi - \eta\ |$ is not small, one has (for $\xi < 1$) the asymptotic expansions

$$S(\xi, \eta) = [b_0 + b_1(\eta)(\xi - \eta) + b_2(\eta)(\xi - \eta)^2 + \cdots]\frac{k(\eta)}{\sqrt{\xi - \eta}}, \tag{8}$$

$$V(\xi, \eta) = [c_0 + c_1(\eta)(\eta - \xi) + c_2(\eta)(\eta - \xi)^2 + \cdots]k(\eta)\sqrt{\eta - \xi}, \tag{9}$$

where $b_0 = 1/\sqrt{2\pi}$, $c_0 = \sqrt{8/\pi}$; $b_1(\eta)$, $c_1(\eta)$, $b_2(\eta)$,..., are nondimensional smooth continuous functions which can be determined from LEFM (for example by optimum fitting of (8) and (9) to finite element results).

3. Superposition of the fields of smeared crack tips

Let us now turn attention to nonlinear fracture mechanics of a cohesive line crack with a nonlinear fracture process zone of nonzero length. The solid is still assumed to be elastic, and the nonlinearity arises only from the relation between the crack bridging stress σ and the crack opening displacements v (the width of the opened crack is denoted as $2v$). Now the basic idea is that the opening profile $v(x)$ of such a crack can be obtained as a sum of the opening profiles of infinitely many LEFM cracks with tips at s that have infinitely small stress intensity factors $dK(s) = k(\eta)dP(s)/b\sqrt{L}$ (where $\eta = s/L$). The tips of these cracks (located at coordinates s) are continuously distributed (smeared) along the crack line (x is also the crack length coordinate); see Fig. 1b, c.

Let $P(\eta) = p(\eta)bL$ be the load corresponding to one LEFM crack whose crack tip has the coordinate $\eta = s/L$; $p(\eta)$ represents the density of the loads with respect to the relative crack tip coordinate $\eta = s/L$. Now a singularity of function $p(\eta)$ needs to be taken into account

in a manner that does not impair accuracy of numerical solutions. The solutions $p(\eta)$ must evidently yield K values that agree with the crack propagation criterion. Thus the value of K is nearly constant for a sufficiently small interval near the tip of the notch in the initial traction-free crack. For constant K, (1) indicates that $P \sim 1/k(\eta)$. For very small η (near the notch tip), $k(\eta) \sim \eta^{1/2}$ (as LEFM solutions for various geometries confirm). Consequently, we must have $p(\eta) \sim \eta^{-1/2}$ near the notch tip. So there is a singularity at $\eta = 0$ which cannot be accurately captured in a finite difference scheme. Therefore, we set $p(\eta) = f(\eta)/\sqrt{\eta}$ where $f(\eta)$ is an unknown function that is nonsingular, and then

$$P(\eta) = bL\frac{f(\eta)}{\sqrt{\eta}}. \tag{10}$$

The load contribution due to the crack tip located within an infinitesimal segment $\mathrm{d}\eta$ with a center at coordinate η is $dP = bL\eta^{-1/2}f(\eta)\,\mathrm{d}\eta$ (keep in mind that all these load contributions dP are applied at the same point as the actual applied load P). By superposition,

$$\sigma(\xi) = \int_0^{\xi} S(\xi, \eta)\eta^{-1/2}f(\eta)\,\mathrm{d}\eta, \tag{11}$$

$$v(\xi) = \frac{L}{E'}\int_{\xi}^{1} V(\xi, \eta)\eta^{-1/2}f(\eta)\,\mathrm{d}\eta. \tag{12}$$

To satisfy equilibrium, the sum of all the load components dP corresponding to all the segments ds must be equal to the applied load P, i.e.

$$P = bL\int_0^1 \eta^{-1/2}f(\eta)\,\mathrm{d}\eta. \tag{13}$$

The load-point displacement corresponding to the crack tips located within segment ds centered at s is $du = \chi(\eta)\eta^{-1/2}f(\eta)L/E'$. Superposition of all these displacement contributions (which all occur at the load application point) yields

$$u = \frac{L}{E'}\int_0^1 \chi(\eta)\eta^{-1/2}f(\eta)\,\mathrm{d}\eta. \tag{14}$$

The meaning of (11–13) is basically equivalent to the equations presented by Planas and Elices ([2] Eqns. (11–13)).

The foregoing formulation can be combined with an arbitrary nonlinear and time-dependent relation between the crack bridging stress σ and the opening displacement v. The stress-displacement law for the fracture process zone (Fig. 2) can be written in the following form:

$$\sigma = F(v, \dot{v}). \tag{15}$$

The superior dot denotes a partial derivative with respect to time t, and F is a given function that characterizes the material and describes both the instantaneous nonlinear response and the rate effect on fracture. Substitution of (11–12) into (15) now yields

$$\int_0^{\xi} S(\xi, \eta)\frac{f(\eta, t)}{\sqrt{\eta}}\,\mathrm{d}\eta = F\left[\frac{L}{E'}\int_{\xi}^{1} V(\xi, \eta)\frac{f(\eta, t)}{\sqrt{\eta}}\,\mathrm{d}\eta, \frac{L}{E'}\int_{\xi}^{1} V(\xi, \eta)\frac{\dot{f}(\eta, t)}{\sqrt{\eta}}\,\mathrm{d}\eta\right]. \tag{16}$$

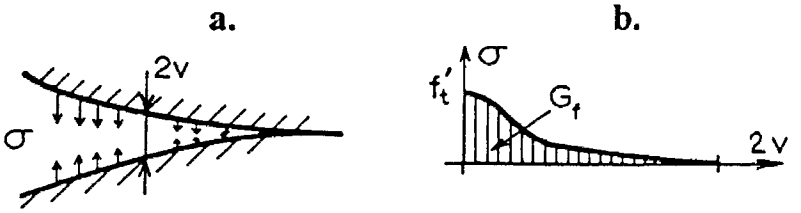

Fig. 2. Crack bridging stresses (cohesive stresses) and stress displacement relation.

This is a singular integro-differential equation for function $f(\eta, t)$. If $\sigma(\xi)$ and $v(\xi)$ were known, then the unknown function $f(\xi, t)$ could be solved from this equation. But $\sigma(\xi)$ and $v(\xi)$ are unknown, and so (16), (14), (11) and (12) are coupled.

4. Method of solution by finite differences

Let us now consider a finite difference solution. Time t is subdivided by discrete times t_r $(r = 1, 2, \dots)$ into small time steps $\Delta t = t_r - t_{r-1}$. The spatial coordinate ξ is subdivided by points $\xi_i = (i-1)\Delta\xi$ $(i = 1, 2, \dots, N+1)$ into N small intervals $\Delta\xi = 1/N$ (Fig. 3). The second-order finite difference approximations for the stresses and displacements written for the center points $\xi_{i+(1/2)} = \xi_i + \frac{1}{2}\Delta\xi$ of intervals $\Delta\xi = \xi_{i+1} - \xi_i$ and for the middle of time step $\Delta t = t_r - t_{r-1}$ are:

$$\bar{\sigma}_{1+(1/2)} = \frac{1}{\sqrt{3\pi}} k(\xi_{1+(1/4)}) \bar{f}_{1+(1/4)} \quad \text{for} \quad i = 1, \tag{17}$$

$$\begin{aligned} \bar{\sigma}_{i+(1/2)} = {} & 2\sqrt{\Delta\xi} S(\xi_{i+(1/2)}, \xi_{1+(1/2)}) \bar{f}_{1+(1/2)} + \\ & + \Delta\xi \sum_{j=2}^{i-1} \left[S(\xi_{i+(1/2)}, \xi_{j+(1/2)}) \frac{\bar{f}_{j+(1/2)}}{\sqrt{\xi_{j+(1/2)}}} \right] \\ & + \sqrt{\frac{\Delta\xi}{\pi}} \frac{k(\xi_{i+(1/4)}) \bar{f}_{i+(1/4)}}{\sqrt{\xi_{i+(1/4)}}} \quad \text{for } i = 2, \dots, N, \end{aligned} \tag{18}$$

$$\begin{aligned} \bar{v}_{i+(1/2)} = {} & \frac{L}{E'} \left[\frac{2}{3\sqrt{\pi}} \frac{\Delta\xi^{3/2} k(\xi_{i+(3/4)}) \bar{f}_{i+(3/4)}}{\sqrt{\xi_{i+(3/4)}}} + \right. \\ & \left. + \Delta\xi \sum_{j=i+1}^{N} V(\xi_{i+(1/2)}, \xi_{j+(1/2)}) \frac{\bar{f}_{j+(1/2)}}{\sqrt{\xi_{j+(1/2)}}} \right] \quad \text{for } i = 1, \dots, N, \end{aligned} \tag{19}$$

$$\begin{aligned} \dot{v}_{i+(1/2)} = {} & \frac{L}{E'\Delta t} \left[\frac{2}{3\sqrt{\pi}} \frac{\Delta\xi^{3/2} k(\xi_{i+(3/4)}) \Delta f_{i+(3/4)}}{\sqrt{\xi_{i+(3/4)}}} + \right. \\ & \left. + \Delta\xi \sum_{j=i+1}^{N} V(\xi_{i+(1/2)}, \xi_{j+(1/2)}) \frac{\Delta f_{j+(1/2)}}{\sqrt{\xi_{j+(1/2)}}} \right] \quad \text{for } i = 1, \dots, N, \end{aligned} \tag{20}$$

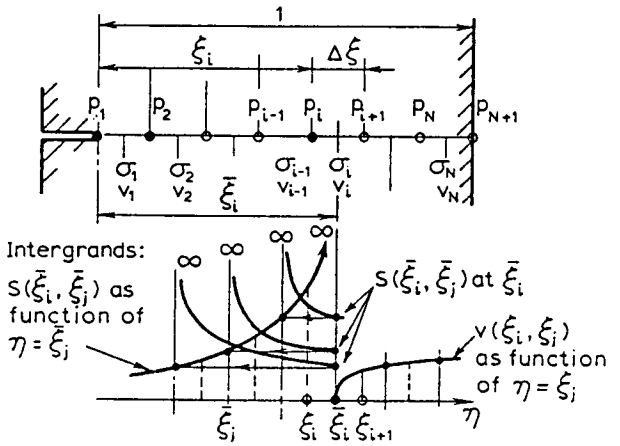

Fig. 3. Discrete subdivision of crack ligament and functions characterizing the distribution of crack opening displacements and stresses along the crack line.

where subscripts i refer to discrete coordinates ξ_i; $\xi_{i+(1/4)} = \xi_i + \frac{1}{4}\Delta\xi$, $\xi_{i+(3/4)} = \xi_i + \frac{1}{4}3\Delta\xi$, and

$$\bar{f}_{i+(1/2)} = \tfrac{1}{2}(\bar{f}_i + \bar{f}_{i+1}), \quad \bar{f}_{i+(1/4)} = \tfrac{1}{4}(3\bar{f}_i + \bar{f}_{i+1}), \quad \bar{f}_{i+(3/4)} = \tfrac{1}{4}(\bar{f}_i + 3\bar{f}_{i+1}), \tag{21}$$

Δf denotes changes of f over the time interval Δf. The overbars refer to the values at the middle of the time step, i.e. at time $t_{r-(1/2)} = t_r - \frac{1}{2}\Delta t$, and Δf denotes the increment over the time step, that is

$$\begin{aligned} &\bar{f}_i = \tfrac{1}{2}(f_i + f_i^{r-1}), \quad \Delta f_{j+(1/2)} = \tfrac{1}{2}(f_j + f_{j+1}) - \tfrac{1}{2}(f_j^{r-1} + f_{j+1}^{r-1}), \\ &\Delta f_{i+(3/4)} = \tfrac{1}{4}(f_i + 3f_{i+1}) - \tfrac{1}{4}(f_i^{r-1} + 3f_{i+1}^{r-1}), \end{aligned} \tag{22}$$

f_i represents the unknown values at the end of the current time step (i.e. at time $t_r = t_{r-1} + \Delta t$), and f_i^{r-1} represents the known values at the end of the preceding time step (i.e. at time t_{r-1}). Superscripts r for the end of the current time step are here omitted, and an overbar is equivalent to superscript $r - \frac{1}{2}$. It is understood that the sums are zero when the upper limit is less than the lower limit of the sum. In deriving (17–19), the integrals in the near-tip and near-notch regions have been integrated as follows

$$\begin{aligned} &\int_{\xi_i}^{\xi_{i+(1/2)}} (\xi_{i+(1/2)} - \eta)^{-1/2}\, d\eta = \sqrt{2\Delta\xi}, \\ &\int_{\xi_{i+(1/2)}}^{\xi_{i+1}} (\eta - \xi_{i+(1/2)})^{1/2}\, d\eta = \tfrac{2}{3}(\tfrac{1}{2}\Delta\xi)^{3/2} \\ &\int_0^{\xi_{1+(1/2)}} [\eta(\xi_{1+(1/2)} - \eta)]^{-1/2}\, d\eta = \pi \end{aligned} \tag{23}$$

Equation (15) must be satisfied for every point $\xi_{i+(1/2)}$, which may be written as

$$\Phi_i = \sigma_{i+(1/2)} - F(v_{i+(1/2)}, \dot{v}_{i+(1/2)}) = 0 \quad (i = 1, \ldots, N). \tag{24}$$

Equation (14) for the prescribed load-point displacement may be approximated in finite difference form as

$$\Phi_{N+1} = \gamma \left[u - \frac{L}{E'} \sum_{j=1}^{N+1} c_j \chi(\xi_j) \frac{f_j}{\sqrt{\xi_j}} \right] = 0, \tag{25}$$

where u and f_j are the values at the end of the current time step (i.e. at time t_r); γ is a chosen scaling parameter introduced for numerical purposes; and c_j represent the coefficients of the numerical integration formula chosen to evaluate the integral in (14).

Equation (13) for load P at the end of the current time step (i.e. at time t_r) may be approximated in finite difference form as

$$P = bL\Delta\xi \sum_{j=1}^{N} c_j \frac{f_j}{\sqrt{\xi_j}}. \tag{26}$$

If the value of displacement u at the end of the time step is prescribed, (24) and (25) represent a system of $N + 1$ nonlinear algebraic equations for the unknowns $f_1, f_2, \ldots, f_{N+1}$. They may be effectively solved by a standard computer library optimization subroutine for the Levenberg–Marquardt algorithm, which minimizes the sum $\Sigma_1^{N+1}\Phi_i^2$. When the minimum of zero is attained, $\Phi_1 = \cdots = \Phi_{N+1} = 0$. Subroutines for calculating the values of $\Phi_1, \ldots, \Phi_{N+1}$ from $f_1, \ldots, f_{N+1}$ based on (24), (25), (17–21) must be written, for being called repeatedly by the optimization subroutine. The initial values of f_i for the optimization process must also be supplied.

In programming the subroutines that calculate functions Φ_i, one must take into account that $v_{i+(1/2)} = 0$ until the stress corresponding to $v_{i+(1/2)}$ for the first time reaches the limit stress at which the crack opening begins. This is achieved by setting $\Phi_i = \gamma' v_{i+(1/2)}$ until this condition is reached (where γ' is a suitably chosen scaling parameter).

With arbitrary initial values, the optimization algorithm would not normally converge to the correct solution, or the convergence would be very slow. However, correct and rapid convergence can be easily achieved by using a small enough time step Δt and supplying to the optimization algorithm, as the initial values, the values $f_i^{r-1} (i = 1, \ldots, N + 1)$ obtained for the end of the preceding time step.

Another important feature is to specify a proper value of parameter γ. If $\gamma = 1$ were used, the values of Φ_{N+1} could differ from the average of the values of $\Phi_1, \ldots, \Phi_N$, by many orders of magnitude depending on the choice of units of measurement. Then either Φ_{N+1}^2 would be negligible compared to $\Phi_1^2 + \cdots + \Phi_N^2$ or vice versa. The problem would be ill-conditioned, the surface of $\Sigma\phi_i^2$ would be cylindrical, and the algorithm would not converge properly. To achieve that Φ_{N+1} be of the same order of magnitude, one may set

$$\gamma = f_t'/u_p, \tag{27}$$

where f_t' = tensile strength of the material and u_p = expected approximate value of u at the peak load. Similarly, one may chose $\gamma' = \gamma$.

5. Generalization to aging viscoelastic material

For materials such as concrete, we must model not only the rate effect in the fracture process zone, but also creep in the entire structure. The stresses outside the fracture process zone may

be assumed to be within the linear viscoelastic range. Then we may consider the stress-strain relation for concrete to be of the form

$$\epsilon(t) = \boldsymbol{B} \int_0^t J(t,\, t')\, \mathrm{d}\sigma(t'), \tag{28}$$

where ϵ and σ are 6×1 column matrices of stress and strain components, $\boldsymbol{B}$ is a constant 6×6 matrix implementing the conditions of material isotropy, and $J(t,\, t')$ is the compliance function representing the strain at age t caused by a unit uniaxial stress acting from age t' to age t. In terms of discrete times $t_0,\, t_1\, , \ldots,\, t_r$ (which do not have to be distributed uniformly in time), we may approximate the history integral in (28) by a finite sum (see, e.g., Bažant [6]):

$$\epsilon^r = \boldsymbol{B} \sum_{q=1}^{r} J_{r,q}(\sigma^q - \sigma^{q-1}), \quad J_{r,q} = J\left(t_r,\, \frac{t_{q-1} + t_q}{2}\right), \tag{29}$$

where superscripts r and q refer to times t_r and t_q.

It may now be noted that the elastic stress-strain relation $\epsilon = \boldsymbol{B}\sigma / E'$ can be transformed into (29) by replacing $1/E'$ with the difference operator

$$\underline{E}^{-1}(\ldots) = \sum_{q=1}^{r} J_{r,q}[(\ldots)^q - (\ldots)^{q-1}]. \tag{30}$$

The linear creep law now permits making this replacement in all the equations of the aforementioned algorithm that contain $1/E'$. These are (19) and (20), and we notice that this operator acts on the variables $f_{j+(1/2)}$ and $f_{i+(3/4)}$. Therefore, it is convenient to define the creep-transformed variables

$$\begin{aligned} g^r_{j+(1/2)} &= \underline{E}^{-1} f^r_{j+(1/2)} = \sum_{q=1}^{r} J_{r,q}(f^q_{j+(1/2)} - f^{q-1}_{j+(1/2)}), \\ g^r_{i+(3/4)} &= \underline{E}^{-1} f^r_{i+(3/4)} = \sum_{q=1}^{r} J_{r,q}(f^q_{i+(3/4)} - f^{q-1}_{i+(3/4)}). \end{aligned} \tag{31}$$

The creep transforms of (19) and (20) may be written as follows

$$\begin{aligned} \bar{v}_{i+(1/2)} = v^{r-(1/2)}_{i+(1/2)} = L \Bigg[& \frac{\Delta\xi^{(3/2)} k(\xi_{i+(3/4)})}{\sqrt{\xi_{i+(3/4)}}} \frac{(g^{r-1}_{i+(3/4)} + g^r_{i+(3/4)})}{3\sqrt{\pi}} + \\ & + \Delta\xi \sum_{j=i+1}^{N} \frac{V(\xi_{i+(1/2)},\, \xi_{j+(1/2)})}{\sqrt{\xi_{j+(1/2)}}} \frac{(g^{r-1}_{j+(1/2)} + g^r_{j+(1/2)})}{2} \Bigg], \end{aligned} \tag{32}$$

$$\begin{aligned} \dot{v}_{i+(1/2)} = \dot{v}^{r-(1/2)}_{i+(1/2)} = \frac{L}{\Delta t} \Bigg[& \frac{2}{3\sqrt{\pi}} \frac{\Delta\xi^{(2/3)} k(\xi_{i+(3/4)})}{\sqrt{\xi_{i+(3/4)}}} (g^r_{i+(3/4)} - g^{r-1}_{i+(3/4)}) + \\ & + \Delta\xi \sum_{j=i+1}^{N} \frac{V(\xi_{i+(1/2)},\, \xi_{j+(1/2)})}{\sqrt{\xi_{j+(1/2)}}} (g^r_{j+(1/2)} - g^{r-1}_{j+(1/2)}) \Bigg], \end{aligned} \tag{33}$$

where $\bar{v}_{i+(1/2)}$ and $\dot{v}_{i+(1/2)}$ now also represent creep transforms.

If we are solving the unknowns at time t_r, all the values for times t_0, t_1 ,..., t_{r-1} are already known. Thus the system of $N + 1$ equations $\Phi_i = 0$ contains $N + 1$ unknowns f_1^r ,..., f_{N+1}^r, and the values of Φ_i can be calculated from f_1^r ,..., f_{N+1}^r using (17), (31), (32), (21), (24) and (25). Again, a subroutine to do this calculation must be provided to the Levenberg–Marquardt optimization algorithm which minimizes $\Sigma\Phi_i^2$. So the solution can proceed in time steps in the same manner as before. The values for time t_{r-1} are used as the initial values for the optimization algorithm that calculates the values at time t_r. The only difference is that all the values of $f_{j+(1/2)}^q$, $f_{i+(3/4)}^q$, $g_{j+(1/2)}^q$, $g_{i+(3/4)}^q$, for times $q = 0, 1, \ldots, r-1$ must now be stored in the computer memory and sums over these values must be repeatedly calculated (while in absence of creep all the values prior to time t_{r-1} can be discarded).

It should be noted that the subdivision of time by t_q need not be uniform. For the case of constant load, the times steps $t_r - t_{r-1}$ should be increased in a geometric progression (i.e. so that they be constant in the log-time scale).

6. Application to nonlinear rate-dependent fracture tests of concrete

The smeared-tip superposition method represents an effective way to model the recent test results of Bažant and Gettu [7], in which three-point-bend fracture specimens were tested over a broad range of loading rates, characterized by time to peak t_p which ranged from 1 s to 300,000 s (this represents a range of over 5 orders of magnitude). The size effect method (RILEM [8]) has been used for determining the fracture energy of the material G_f and the effective length of the fracture process zone c_f, and particularly their dependence on the loading rate. For the purpose of the size effect method, geometrically similar specimens of three different sizes, with size ratios 1 : 2 : 4, have been tested for every loading rate. The specimens were three-point-bend beams of depths $d = 38$, 76, 152 mm, span $2.5d$ and notch depth $\frac{1}{6}d$. The details of the test procedure and the test results are given in [7] and need not be repeated here. Various consequences of these tests are discussed in Bažant and Jirásek [9], in which a rate dependent R-curve model with creep has been presented and shown to model the test results well. The R-curve approach, however, does not have a general validity since the R-curves depend on the specimen shape. Therefore a more fundamental analysis of these test results in terms of a crack with bridging stresses is desirable. The present formulation of the smeared-tip method is suitable for this purpose.

The test results revealed a strong dependence of the peak load and post-peak response on the loading rate, which is apparent from Fig. 4. The response curves correspond to a constant rate of the crack-mouth opening displacement (CMOD). Based on the maximum load for similar specimens of different sizes, the size effect plots based on the size effect law proposed in 1984 by Bažant (see, e.g. [1]) have been constructed from the test results (see [7]).

A surprising feature of these test results has been a shift to a higher brittleness at decreasing loading rate (i.e. shift toward LEFM-type behavior). This shift of brittleness appeared difficult to model, nevertheless a material fracture law that yields this shift of brittleness has been found by trial-and-error approach. After examining many different material fracture laws, the following law has been found to fit the test results of [7] adequately and generally exhibits the basic known trends of rate dependent fracture behavior

$$\sigma(v, \dot{v}) = s(v) + S(v, \dot{v}), \tag{34}$$

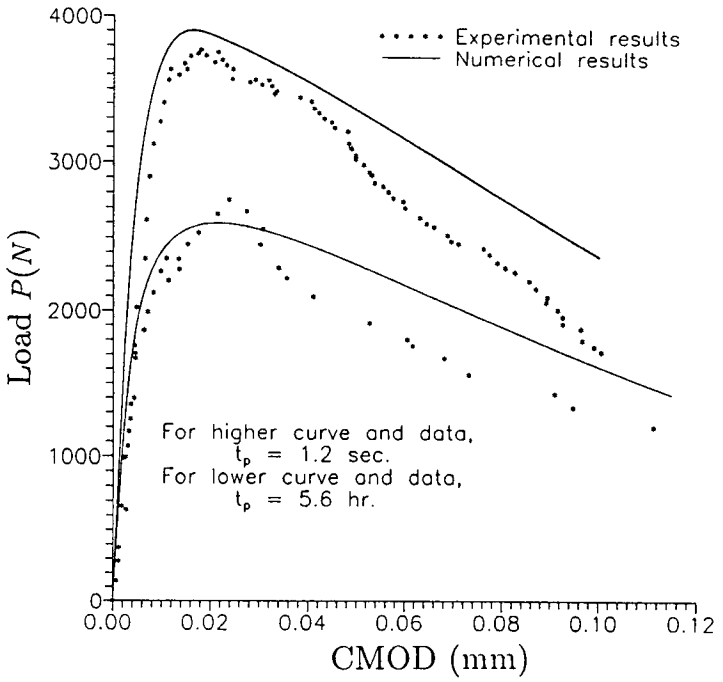

Fig. 4. Example of test results of [8] for two different loading rates, and comparison with calculated curves.

in which

$$s(v) = b(a + v^{0.5}) \exp(-cv), \tag{35}$$

$$S(v, \dot{v}) = f_t' \rho \left[1 - \frac{f_t'}{\omega G_f} v\right] \left[1 - \exp\left(\frac{-\dot{v}}{\dot{v}_r}\right)\right] \quad \text{if } > 0; \text{ else } 0. \tag{36}$$

Here G_f, $\dot{v}_r$, ω, ρ, a, b, and c are empirical constants, whose physical dimensions are obvious. f_t' is the tensile strength of the material, which is introduced only for the purpose of dimensionality and is determined by other types of tests.

As (34) indicates, the behavior in the fracture process zone is characterized by the rheologic model in Fig. 5 in which a viscous element is coupled in parallel with a cracking element. The cracking element describes progressive cracking at increasing displacement v, as characterized by (35). The viscous element is described by (36) and obviously corresponds to a viscosity that is dependent on the rate of separation $\dot{v}$ as well as the magnitude of separation v. In (35) (Fig. 6), the parameters a, b, and c are determined so that:

(1) $s(0) = \alpha f_t'$ where α is a specified fraction of strength f_t';
(2) the peak stress is f_t'; and
(3) the area under the curve is $\frac{1}{2} G_f$.

This means that among parameters a, b, c only one is independent. The parameters ρ and ω control the magnitude of viscosity and the degree of separation up to which the viscosity acts. Parameter $\dot{v}_r$ controls the extent to which the rate of separation affects the bridging stress.

With regard to the rheologic model in Fig. 5, it should be noted that a linear viscous element cannot be used to represent the available test data realistically, neither in parallel coupling nor

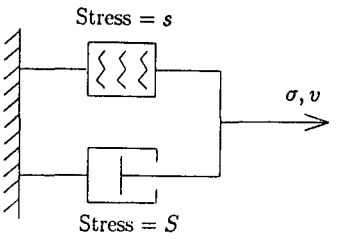

Fig. 5. Rheologic model for the softening stress-displacement relation for a crack.

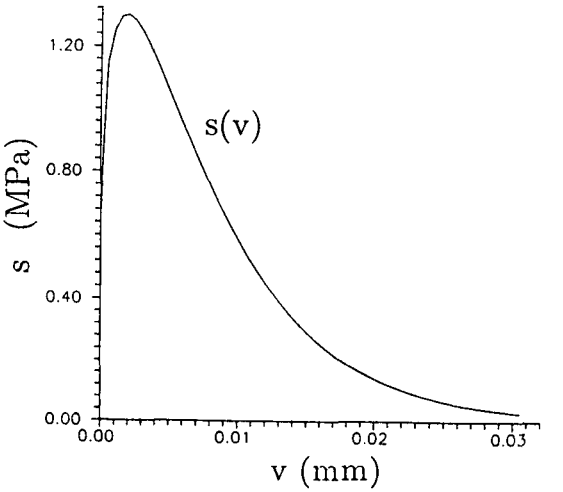

Fig. 6. Dependence of the crack bridging stress at constant opening displacement rate.

in series coupling. For the case of a constant viscosity (independent of the displacement and displacement rate), the values of the peak load for different rates also differed by an order of magnitude, which grossly disagrees with test results. A highly nonlinear viscous element is inevitable to model the fact that a change of loading rate by 5 orders of magnitude changes the peak stress by less than 100 percent.

The fitting of the test results of Bažant and Gettu resulted in the following values of the empirical material parameters: $\rho = 2$, $\omega = 0.65$, $\dot{v}_i = 0.012\,\text{mm/day}$, and $\alpha = 0.5$ with $f'_t = 1.3$ MPa. The fracture energy was obtained as $G_f = 2.0 \times 10^{-6}\,\text{J/m}^2$.

The compliance function of concrete in the bulk of the specimen has been characterized by the double-power law ([6], p. 157), which works particularly well for creep durations less than about 1 week. According to this law

$$J(t, t') = \frac{1}{E_0} + \frac{\phi_1}{E_0}(t'^{-m} + \alpha_1)(t - t')^n, \tag{37}$$

in which E_0, ϕ_1, m, n, and α_1 are material parameters. For the purpose of characterizing the specimens tested, the following values have been identified: $E_0 = 9.42$, $\phi_1 = 0.711$, $m = 0.315$, $n = 0.12$, $\alpha_1 = 0.0417$.

For the three-point-bend specimen geometry used, with span-to-depth ratio $L/d = 2.5$, the following function characterizing the stress intensity factor, (1), determined on the basis of finite element results, [1], has been used:

$$k(\alpha) = 3.75\sqrt{\pi\alpha}(1 - \alpha)^{-3/2}(1 - 1.25\alpha + 4.49\alpha^2 - 3.98\alpha^3 + 1.33\alpha^4), \tag{38}$$

where $\alpha = a/d = (\eta + a_0/L)/(1 + a_0/L)$, $\eta = s/L$, $a = a_0 + s$ = total crack length (with the notch), and $d = a_0 + L$ = beam depth. Some of the load-displacement curves obtained with the present model are shown by the solid curves in Fig. 4, in comparison with the test results. It is seen that the strong effect of the loading rate on the peak stress and post-peak response is modeled sufficiently well.

Figure 7 shows the size effect plot obtained from a group of specimens of three different sizes at different loading rates. The coordinate in this plot is $\log \beta$, where $\beta = d/d_0$ = relative

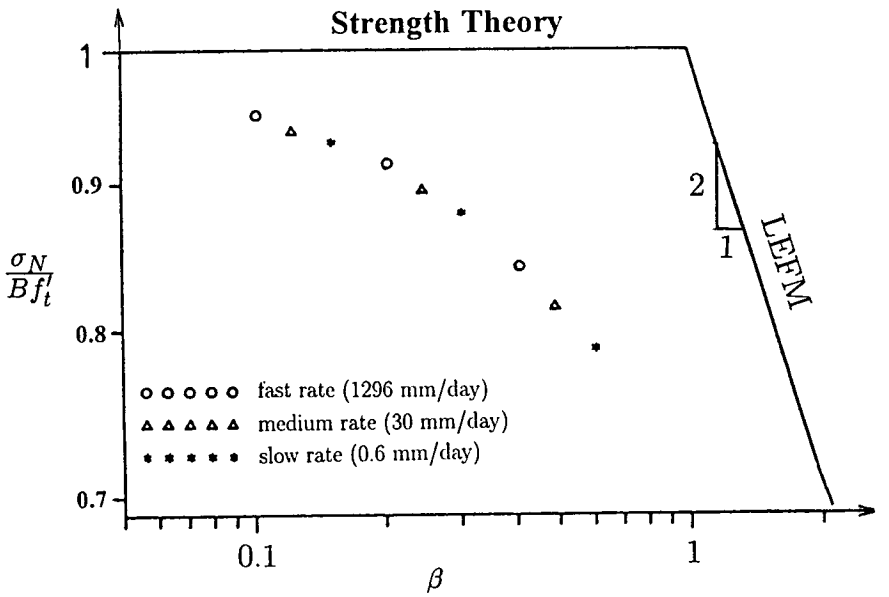

Fig. 7. Size effect plot obtained for three specimen sizes and three different loading rates.

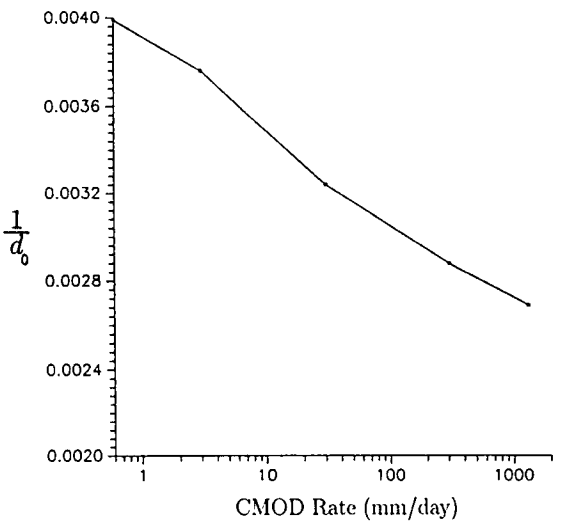

Fig. 8. Variation of transitional size d_0 of the size effect law with the loading rate.

size, d_0 = constant, and the ordinate in this plot is $\log(\sigma_N/Bf'_t)$, where $\sigma_N = P/bd$, b = specimen thickness (same for all the sizes in these tests) and d = characteristic dimension of the specimen = depth of the beam. The failures governed by strength theory yield in this plot a horizontal line, while the failures obeying linear elastic fracture mechanics give an inclined straight line of slope $-\frac{1}{2}$ shown in the plot. The transitional behavior indicates nonlinear fracture behavior with a large fracture process zone.

The maximum loads P for specimens of various sizes and for various loading rates have been calculated with the present model, and from them the nominal strengths have been

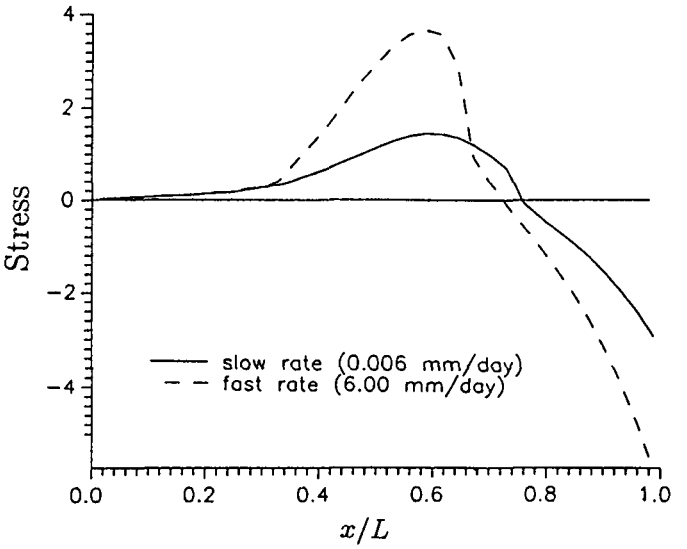

Fig. 9. Stress profiles.

evaluated. The values of nominal strength have been analyzed by linear regression according to the size effect law proposed by Bažant, as described for example in [7]. These regressions yielded for each loading rate the value of d_0.

Now an important result to note is that, in agreement with experiments, the value of d_0 increases as the loading rate increases (Fig. 8). This causes the group of specimens for the three different sizes to shift in the size effect plot to the right as the loading rate decreases, i.e. the response is becoming more brittle (closer to LEFM). Qualitatively, the prediction of the present model shown in Fig. 7 agrees with this experimentally observed trend. Close fitting, however, has not been attempted because the purpose of the present investigation has been mainly to verify the smeared-tip method and demonstrate its application rather than to model the test results. Anyway, a complete mathematical model for the fracture process cannot be obtained solely on the basis of the tests of Bažant and Gettu since further information is needed on the response of the specimens to sudden change of the loading rate by several orders of magnitude, and on the stress relaxation in the process zone. An ongoing experimental study will generate test data on this behavior (Bažant, Gu and Faber [10]), and once this study is completed a refined mathematical model for the fracture process can be calibrated.

A further illustration of the predictions of the present model is seen in Fig. 9 which shows the stress profiles calculated for the instant when CMOD = 0.04 mm, for very different loading rates. As expected, the stress profiles are very different. Reduction of the loading rate generally causes a reduction of the stresses in the process zone.

7. Conclusions

1. A crack of an arbitrary profile can be represented as the superposition of infinitely many smeared LEFM cracks with infinitely small stress intensity factors. Knowledge of the stress intensity factor as a function of the crack tip location along the known crack path is all that is needed for calculating the load-displacement curve of the specimen or structure.
2. The formulation leads to a singular integral equation between the load and the load-point displacement. This equation is supplemented by the stress-displacement relation for the crack opening, which can be rate independent or rate dependent.

3. When the material in the bulk of the specimens exhibits linearly viscoelastic creep, application of the creep operator method yields a two-dimensional integral equation in space and time which also involves integrals over the previous history of the crack opening displacement profiles.
4. If the singularities in the kernels of the integral equations are properly taken into account, the numerical solution of the problem can be obtained by the finite difference method, in which the crack path is subdivided into small intervals. Furthermore, a discrete subdivision of time into loading steps can be used to obtain the response by the technique of incremental loading, with the history integrals for creep approximated by finite sums. This reduces the problem to a system of nonlinear algebraic equations. These can be solved, for example, by a nonlinear optimization algorithm, in which the crack opening profile calculated in the preceding load step is used as an initial estimate for the optimization process in the current loading step.
5. Application of the method is demonstrated for the case of rate-dependent response of geometrically similar three-point-bend fracture specimens of different sizes. The calculated response is qualitatively similar to the previously obtained test results. (Formulation of a definitive mathematical model for the fracture process is planned for future study and is not attempted here because further test results are needed to make unambiguous interpretation of test data possible.)

Acknowledgments Partial financial support under AFOSR Grant No. 91-0140 to Northwestern University, monitored by Dr. J.C.I. Chang, is gratefully acknowledged. Further partial support for the conduct of the experiments analyzed here has been obtained from the Center for Advanced Cement-Based Materials at Northwestern University. Thanks are due to Dr. Jaime Planas, visiting scholar at Northwestern University (on leave from Technical University, Madrid), for some very helpful discussions.

References

1. Z.P. Bažant, *Mechanics Research Communications* 17,5 (1990) 343–351.
2. J. Planas and M. Elices, *Anales de Mecánica de la Fractura (Madrid)* No. 3 (1986) 219–227.
3. J. Planas and M. Elices, 'Asymptotic analysis of the development of a cohesive crack zone in mode I loading for arbitrary softening curves', Internal report, Department of Physics, Universidad Politecnica de Madrid (1987).
4. D. Broek, *Elementary Engineering Fracture Mechanics*, Martinus Nijhoff, Dordrecht (1986).
5. Z.P. Bažant and L. Cedolin, *Stability of Structures: Elastic, Inelastic and Fracture Theories*, Oxford University Press, New York (1991).
6. Z.P. Bažant (ed.), *Mathematical Modeling of Creep and Shrinkage of Concrete*, J. Wiley & Sons, New York (1988).
7. Z.P. Bažant and R. Gettu, *ACI Materials Journal* 89,5 (1992) 456–468.
8. Z.P. Bažant, *Materials and Structures* (RILEM, Paris) 23 (1990) 461–465 (submitted by RILEM Committee TC 89-FMT).
9. Z.P. Bažant and M. Jirásek, in *Proceedings, International Conference on Fracture Mechanics of Concrete Structures*, Breckenridge, Colorado, Z.P. Bažant (ed.), Elsevier Applied Science, London (1992) 918–923.
10. Z.P. Bažant, W.-H. Gu and K.T. Faber, *ACI Materials Journal* (1994) in press.